Bioorganic & Medicinal Chemistry 17 (2009) 1244–1250

Contents lists available at ScienceDirect

Bioorganic & Medicinal Chemistry

journal homepage: www.elsevier.com/locate/bmc

Correlation of binding constants and molecular modelling of inhibitors in the active sites of aldose reductase and aldehyde reductase

Vincenzo Carbone [a], Hai-Tao Zhao [a], Roland Chung [a], Satoshi Endo [b], Akira Hara [b], Ossama El-Kabbani [a,*]

[a] Medicinal Chemistry and Drug Action, Monash Institute of Pharmaceutical Sciences, Monash University, 381 Royal Parade, Parkville, Victoria 3052, Australia
[b] Laboratory of Biochemistry, Gifu Pharmaceutical Laboratory, Mitahora-Higashi, Gifu 502-8585, Japan

ARTICLE INFO

Article history:
Received 3 November 2008
Revised 8 December 2008
Accepted 10 December 2008
Available online 24 December 2008

Keywords:
Aldo–keto reductase superfamily
Aldehyde reductase
Aldose reductase
Inhibitor binding
Molecular modelling

ABSTRACT

Aldose reductase (ALR2) belongs to the aldo–keto reductase (AKR) superfamily of enzymes, is the first enzyme involved in the polyol pathway of glucose metabolism and has been linked to the pathologies associated with diabetes. Molecular modelling studies together with binding constant measurements for the four inhibitors Tolrestat, Minalrestat, quercetin and 3,5-dichlorosalicylic acid (DCL) were used to determine the type of inhibition, and correlate inhibitor potency and binding energies of the complexes with ALR2 and the homologous aldehyde reductase (ALR1), another member of the AKR superfamily. Our results show that the four inhibitors follow either uncompetitive or non-competitive inhibition pattern of substrate reduction for ALR1 and ALR2. Overall, there is correlation between the IC_{50} (concentration giving 50% inhibition) values of the inhibitors for the two enzymes and the binding energies (ΔH) of the enzyme–inhibitor complexes. Additionally, the results agree with the detailed structural information obtained by X-ray crystallography suggesting that the difference in inhibitor binding for the two enzymes is predominantly mediated by non-conserved residues. In particular, Arg312 in ALR1 (missing in ALR2) contributes favourably to the binding of DCL through an electrostatic interaction with the inhibitor's electronegative halide atom and undergoes a conformational change upon Tolrestat binding. In ALR2, Thr113 (Tyr116 in ALR1) forms electrostatic interactions with the fluorobenzyl moiety of Minalrestat and the 3- and 4-hydroxy groups on the phenyl ring of quercetin. Our modelling studies suggest that Minalrestat's binding to ALR1 is accompanied by a conformational change including the side chain of Tyr116 to achieve the selectivity for ALR1 over ALR2.

1. Introduction

The polyol pathway of glucose metabolism is often linked to the development of various complications of diabetes, a global and continually growing epidemic.[1,2] These include progressively degenerative pathologies such as peripheral neuropathy,[3] retinopathy,[4] cataract formation,[5] cardiovascular disease[6] and nephropathy in the form of kidney lesions.[7] Aldose reductase (ALR2; EC 1.1.1.21), a ubiquitous protein which has been isolated and purified in the brain, kidney, liver, lens, and skeletal muscle tissue,[8–11] is the first enzyme of the polyol pathway, converting glucose into sorbitol.[12] It is the over-utilisation of this biochemical pathway which has been linked to the tissue-based pathologies associated with diabetes[2] and with the widespread nature of the disease underscoring the potential in the development of a potent aldose reductase inhibitor (ARI), providing an obvious strategy in preventing or delaying the onset of diabetic complications.

ALR2 belongs to the aldo–keto reductase (AKR) superfamily of enzymes responsible for a wide variety of distinct and sometimes overlapping biological functions from synthesis, modification and metabolism of metabolically vital compounds such as steroids[13–16] (including progesterone signalling in breast mammary cells[17]) to facilitating the NADPH-dependent reduction of endogenous and xenobiotic aldehydes and dicarbonyl compounds.[8,18–22] Members of this superfamily are composed of approximately 315–330 residues, and generally form monomeric proteins with a molecular weight of 36 kDa[23,24] adopting an α/β-TIM barrel structure.[25,26]

To date, none of the currently available ARIs have been approved for clinical use (outside of Japan) due to toxicity problems and lack of specificity towards the target enzyme.[27] Recently, we have demonstrated that a number of thoroughly investigated ARIs readily inhibit 3(17)α-hydroxysteroid dehydrogenase (AKR1C21),[28] a member of the AKR superfamily. However, the lack of specificity is due mostly to the degree of structural and sequence (~65%) homology ALR2 shares with another key AKR-aldehyde reductase (ALR1, EC 1.1.1.2).[29] Biochemical, molecular modelling and crystallographic studies have shown that most known ARIs inhibit ALR1 due to the active sites of both enzymes containing common characteristics in the

* Corresponding author. Tel.: +61 3 9903 9691; fax: +61 3 9903 9582.
E-mail address: ossama.el-kabbani@vcp.monash.edu.au (O. El-Kabbani).

0968-0896/$ - see front matter © 2008 Elsevier Ltd. All rights reserved.
doi:10.1016/j.bmc.2008.12.024

manner by which they bind substrate and inhibitor[29,30] including a conserved hydrogen-bonding interaction between the polar pharmacophore of the inhibitor with conserved active-site residues Tyr, His and Trp that line an anionic-binding site.[30–37] Non-conserved residues present at the C-terminal end of the α/β-TIM barrel structure of both enzymes are responsible for the varied substrate specificity[38,39] and account for the difference in inhibitor potency between the two enzymes. Both enzymes catalyse the NADPH-dependent reduction of an assortment of aldehydes, ketones, small sugars,[21,23,24,40–42] and are involved in the detoxification process by removing reactive aldehydes.[43] Whilst the more hydrophobic nature of the active site of ALR2 makes it more suitable to reduce a number of lipid aldehydes,[44] ALR1 has specialised roles in the regulation of the pro-inflammatory response,[45] metabolism of prostaglandins,[46] and detoxication of reactive dicarbonyl compounds such as methylglyoxal and 3-deoxyglucosone.[18,22]

The most potent and thoroughly investigated ARIs are the orally active carboxylic acid-based inhibitors such as Tolrestat and the cyclic imide molecules based on Sorbinil.[2] To correlate enzyme–inhibitor interaction with inhibitor binding constants for ALR1 and ALR2, the active-sites of the enzymes were compared, along with molecular modelling calculations and inhibitory activity measurements. Structurally diverse compounds which are quite potent in vitro such as Tolrestat,[39,47] the cyclic imide- Minalrestat,[35] the phenolic flavonoid– quercetin[48] and the salicylic acid-based compound, DCL, were investigated, with each compound previously identified via crystallographic analysis, with the exception of quercetin, as an inhibitor capable of binding to the active site of either or both ALR2 and ALR1.

2. Results

2.1. Enzyme kinetics

Kinetic analysis revealed uncompetitive inhibition with all ARIs and the reductase activity of ALR2, whilst ALR1 displayed uncompetitive inhibition with Tolrestat and quercetin and mixed levels of competitive and non-competitive inhibition with Minalrestat and

Table 1
Inhibitor binding constants ΔH and IC_{50} values of ALR2 and ALR1 for ARIs

Inhibitor	IC_{50} (μM)		Inhibition pattern		ΔH Total		ΔH Anionic-binding site	
	ALR2	ALR1	ALR2	ALR1	ALR2	ALR1	ALR2	ALR1
Tolrestat	0.26	2.19	U	U	−92.5	−75.7	−43.5	−49.5
Minalrestat	0.28	0.04	U	M	−87.1	−76.6 (−85.3)	−32.0	−33.1
Quercetin	5.92	38.4	U	U	−60.1	−49.1	−26.8	−26.8
DCL	127	11.3[a]	U	M	−31.1	− 46.7	−24.7	−24.2

ΔH values (kcal/mol) for the anionic-binding sites in ALR2 and ALR1 (Tyr48/50, His110/113 and Trp111/114, respectively) are also given.
[a] IC_{50} value reported by Carbone et al.[54] Inhibition pattern is indicated by the letters U and M for uncompetitive and mixed-type inhibition, respectively. ΔH value for Minalrestat given in parentheses was calculated with the model including the proposed change in the side chain conformation of Tyr116 in ALR1.

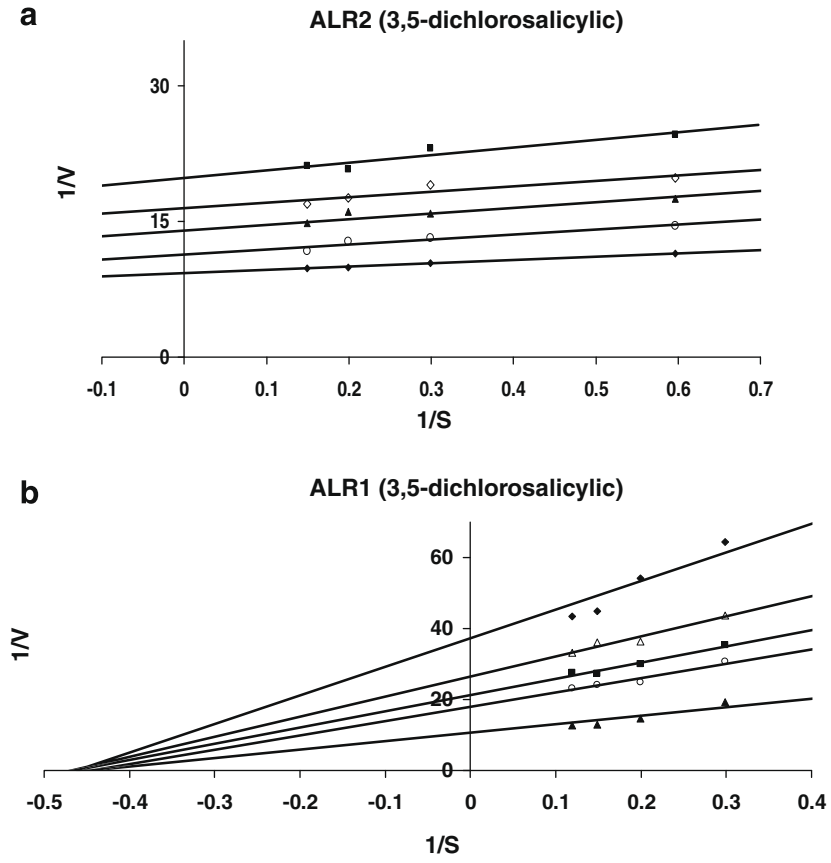

Figure 1. Inhibition patterns of the reductase activities of ALR2 (a) and ALR1 (b) by DCL. DCL concentrations: 150 (■), 75 (◇), 45 (▲), 15 (○) and 0 μM (♦) in (a); and 30 (♦), 15 (△), 11.25 (■), 7.5 (○) and 0 μM (▲) in (b). Converging lines indicate mixed-type of competitive and non-competitive inhibition with respect to substrate, DL-glyceraldehyde (mM), whilst parallel lines indicate uncompetitive inhibition. Velocity is expressed as micromol/min/mL.

DCL (Table 1 and Fig. 1). Based on the IC_{50} (concentration giving 50% inhibition) values, Minalrestat proved to be a 6-fold more potent inhibitor of ALR1 than ALR2, although the IC_{50} of 0.28 μM reported in this study is higher than a previously reported value of 0.07 μM.[49] Like Minalrestat, DCL was a more potent inhibitor of ALR1 (11.3-fold) whilst Tolrestat (8.1-fold) and quercetin (6.5-fold) proved to be better inhibitors of ALR2. These overall kinetic results resemble those from previous evaluations of ARIs[30,47] using various substrates, with the majority of inhibitors displaying similar uncompetitive inhibition in vitro.

2.2. Molecular modelling

The affinity for the bound or modelled inhibitor in either enzyme was further examined via binding energy calculations, utilising the protonation states observed for the inhibitors in previous crystallographic and modelling studies (Scheme 1).[35,50,51] Whilst the inhibitor binding constants (ΔH) were not as sensitive in monitoring inhibitor affinity as well as the IC_{50} values, a change in binding energies is observable and correlates with the varying potencies of inhibitors. The total interaction energies are the largest for the most potent inhibitor of ALR2—Tolrestat (−92.5 kcal, ALR1 −75.7 kcal) and the smallest for the least potent inhibitor—DCL (−31.9 kcal, ALR1 −46.7 kcal). Whilst the sum of the interaction energy provides a strong indication towards inhibitor potency, it is the individual interactions between inhibitor and residue(s) which helps further the understanding of the ARIs mode of inhibition. This includes analysing the substrate-binding pocket, with residues that actively participate in the catalytic mechanism—Tyr48, Lys77 and His110 (corresponding residues are Tyr50, Lys80 and His113, respectively, in ALR1) and the nicotinamide moiety of $NADP^+$ [52,53]. As previously seen in high-resolution crystal structures of ALR2 complexes, Tyr, Lys, and His remain in the protonated state whilst the inhibitor's carboxylate group remains partially deprotonated,[51] providing electrostatic interaction between the enzyme and inhibitor. These inhibitor interactions in total remain almost identical regardless of their selectivity for ALR2 and ALR1 (Table 1). However, in the case of DCL, the inhibitor forms approximately 80% of the total interaction with the catalytic residues of ALR2, indicative of the poorer nature of the inhibitor due to the lack of meaningful interaction with other non- catalytic residues of the active site. The opposite also holds true for the most potent inhibitors. These inhibitors form multiple contacts producing total energy interactions with the catalytic residues that are lower than 50% of the sum interaction and include Tolrestat (ALR2; 47.1%) and Minalrestat (ALR2; 36.8% and ALR1; 43.2%).

2.2.1. DCL

In the crystal structure of ALR1:DCL[54] (Fig. 2a) the inhibitor formed a number of main-chain and side-chain interactions with Trp22, Tyr50, His113, Trp114 and Arg312, all falling within 4 Å of the inhibitor. Arg312 is within hydrogen-bonding distance from the 3-Cl atom of DCL (3.2 Å and 2.7 Å), with a binding energy of −5.5 kcal, whilst the 5-Cl atom forms a hydrogen bond with the side-chain nitrogen (NE1) of Trp22 (3.0 Å, −4.2 kcal). The 2-OH group of DCL forms a hydrogen bond with the side-chain nitrogen (NE1) of Trp114 (3.2 Å), whilst the carboxylate forms a hydrogen bond with the OH of Tyr50 (3.4 Å) and the nitrogen (NE2) of His113 (3.4 Å). The modelled ALR2:DCL complex (Fig. 2b) forms fewer interactions with active site residues. The majority are formed by the carboxylate of DCL with the nitrogen (NE1) of Trp111 (3.7 Å), the nitrogen (NE2) of His110 (3.5 Å) and the hydroxyl (OH) of Tyr48 (3.5 Å). The 5-Cl atom of DCL forms van der Waals contact with the carbonyl of Val47 (2.8 Å) and π stacking interaction with Trp20 (5.4 Å, −5.9 kcal) whilst the bulky Phe122 which occupies the same space as Arg312 in ALR1 falls within 3 Å of the inhibitor but produces an overall dispersive interaction with the molecule.

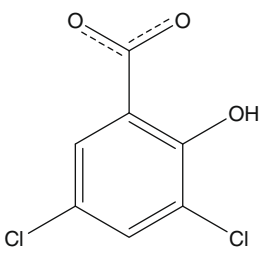

3, 5-Dichlorosalicylic acid (DCL)

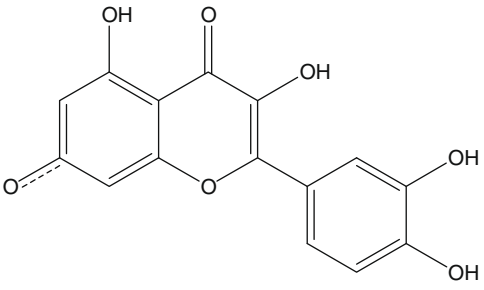

Quercetin

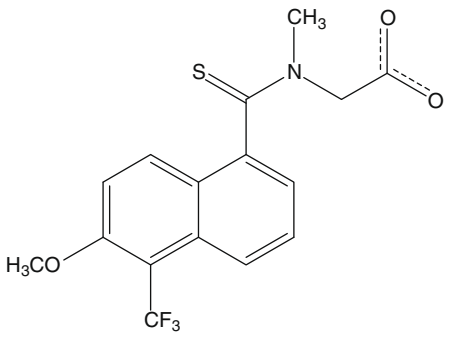

Tolrestat

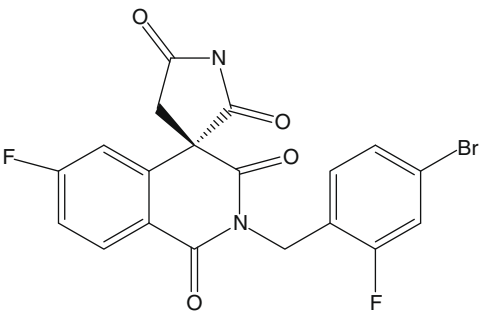

Minalrestat

Scheme 1. Chemical structures of ARIs.

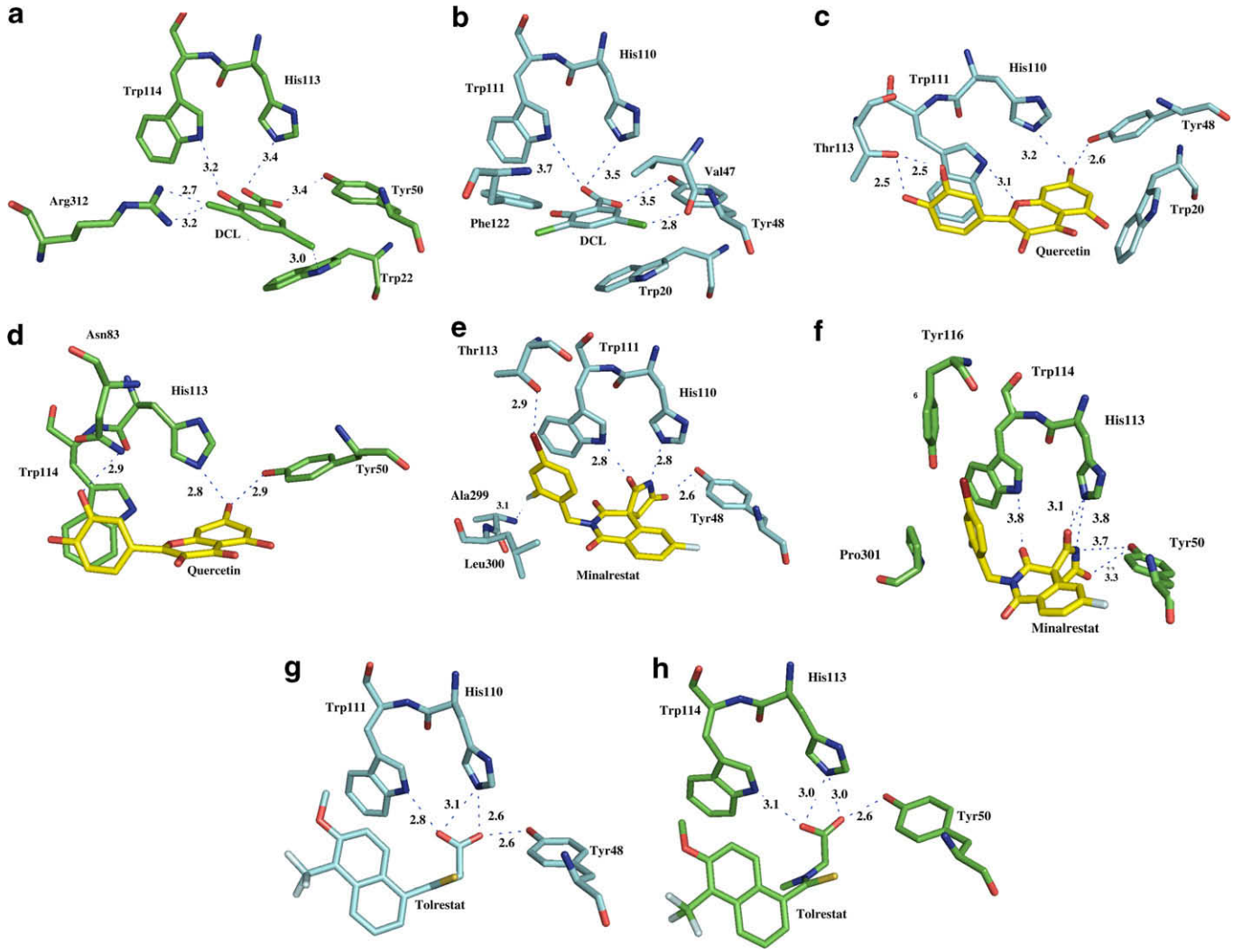

Figure 2. The inhibitor binding sites. (a) ALR1:DCL, (b) ALR2:DCL, (c) ALR2:quercetin, (d) ALR1:quercetin, (e) ALR2:Minalrestat, (f) ALR1:Minalrestat, (g) ALR2:Tolrestat, (h) ALR1:Tolrestat. Residues of the anionic-binding site (Tyr, His and Trp) and residues within 4 Å of ARIs are shown with corresponding hydrogen bonds illustrated as blue dotted lines and distances given in angstroms. Figures were prepared using PyMOL.[62]

2.2.2. Quercetin

The orientation of quercetin within the active site of ALR2 was based on modelling studies of 1-benzopyran-4-one antioxidant derivatives[48] (Fig. 2c). The 7-OH group of quercetin forms hydrogen bonds with the nitrogen (NE2) of His110 (3.2 Å) and the OH of Tyr48 (2.6 Å), whilst the side chain of Thr113 (OG1) forms a hydrogen bond with the 3- and 4-OH groups on the phenyl ring (2.5 Å), producing a binding interaction energy of −5.3 kcal. Trp111 (NE2) forms a hydrogen bond interaction with the benzopyran oxygen (3.1 Å), however it is the π stacking interaction between the 3,4-hydroxyphenyl and the Trp side chain (3.8 Å) that largely contributes to the interaction energy (−12.6 kcal). Similarly in ALR1 (Fig 2d), Trp114 stacks with the same phenyl group (4.0 Å, −11.3 kcal) but fails to make a hydrogen bond contact, whilst the 7-OH group of quercetin forms equivalent hydrogen bonds with His113 (2.8 Å) and Tyr48 (2.9 Å), and the 3-OH group forms a hydrogen bond with the side chain nitrogen (ND2) of Asn83 (2.9 Å). Along with Trp111/114, quercetin makes a large number of additional (and most likely stabilizing) hydrophobic contacts including Trp20, Val47, Trp79, Phe115, Phe122, Leu300 and Tyr309 in ALR2 for a combined interaction energy of −30.3 kcal and in ALR1 Trp22, Trp82, Tyr116, Phe118, Phe125, Trp220 and Pro301 for a combined interaction energy of −29.1 kcal, in excess of the total anionic-binding site interaction for either enzyme (Table 1).

2.2.3. Minalrestat

The crystal structure of ALR2 complexed with Minalrestat has been published[35] (Fig. 2e). The cyclic imide moiety of the inhibitor interacts with the catalytic residues His110 (NE2; 2.8 Å) and Tyr48 (OH; 2.6 Å), and Trp111 (NE1; 2.8 Å), which in addition to the hydrogen bonding, π stacks with the fluorobenzyl group (3.5 Å, −9.6 kcal). Additional hydrogen bonding interactions are formed with Thr113 (OG1; 2.9 Å) and Leu300 (N; 3.1 Å). The isoquinoline ring forms a number of hydrophobic contacts with residues Trp20, Val47, Trp79, Trp111, Phe115, Phe122, Trp219 and Leu300 (−46.4 kcal). In ALR1 (Fig. 2f) the cyclic imide moiety makes similar interactions with the side chain nitrogen (NE2) of His113 (O; 3.1 Å, N; 3.4 Å), the hydroxyl (OH) of Tyr50 (N; 3.7 Å, O; 3.3 Å), and the side chain nitrogen (NE2) of Trp114 (O; 3.8 Å). One significant difference between the ALR2 crystal structure and the ALR1: Minalrestat model is the failure of the fluorobenzyl group to π stack against Trp114 due to steric interference by Tyr116 that would be present within the specificity pocket described for ALR2, where the dispersive interaction of Tyr116 is replaced by the smaller Thr113 and may account for the difference in ΔH for ALR1. The loss in interaction energy between ALR1 and Minalrestat resulting from Tyr116 is partly compensated for by Arg312 (−10.3 kcal). Additionally, the isoquinoline ring of Minalrestat forms a number of hydrophobic contacts with residues Trp22,

Ile49, Trp82, Trp114, Phe118, Phe125, Pro301 and Met302 (−33.3 kcal) of ALR1.

2.2.4. Tolrestat

The crystal structures of ALR2[55] (Fig. 2g) and ALR1[31] (Fig. 2h) complexed with Tolrestat have been published. Like DCL, the carboxylate group of Tolrestat interacts with His110/113 (NE2; ALR2 2.6 Å, 3.1 Å, ALR1 3.0 Å, 3.0 Å), Tyr48/50 (OH; ALR2 2.6 Å, ALR1 2.6 Å) and Trp111/114 (NE1; ALR2 2.8 Å, ALR1 3.1 Å). In ALR1, the side chain torsion angles of Arg312 differ from those in the binary complex and the salt bridge with Asp313 is missing. Overcoming such an interaction to affect binding to the active site may account for the difference in Tolrestat's potency between the two enzymes. In both ALR1 and ALR2, Tolrestat is held firmly by a number of hydrophobic interactions, for ALR2 mediated by Trp20, Val47, Trp79, Trp111, Phe115, Val130, Phe122, Trp219 and leu300 (−51.3 kcal) and for ALR1 Trp22, Ile49, Trp82, Phe118, Phe125, Trp114, Trp220, Ile299, Pro301 and Met 302 (−31.8 kcal). Like the aforementioned quercetin and Minalrestat complexes for either enzyme, the hydrophobic interaction energies for ALR2 are in excess to the total binding energies in the anionic-binding site.

3. Discussion

ALR2 inhibition has been widely studied in vitro with analysis overwhelmingly demonstrating the inhibition of the enzyme by a large number of compounds that are in some cases only several orders of magnitude more potent than for ALR1. It has been demonstrated in a number of animal studies that the inhibition of ALR2 significantly impedes the development or progression of diabetic retinopathy and cataract formation,[56] however these ARIs are not without side effects. In particular, carboxylic acid-containing compounds generally have difficulty in achieving appropriate levels in target tissues, and whilst cyclic imides and their related derivatives appear to adequately reach target tissues, they demonstrate a number of side effects[2] and thus far failed to complete clinical testing or have been abandoned all together. Regardless of the failure of several ARIs to reach a commercial market they remain a strong and important area of focus for the treatment of diabetes.

Porcine ALR1 shares 97% sequence homology and a conserved active-site structure with human ALR1,[57] making structural comparisons between the two enzymes possible. Crystallographic information gathered from ternary complexes of ALR2 or ALR1[54,55,31] makes possible the calculation and analysis of binding energies and molecular interactions between active site residues and ARIs thereby providing an insight for the mechanism of inhibition. High-resolution crystallographic analyses are used to determine the inter-molecular interaction of the enzyme–inhibitor complex and the mechanism of catalysis as they can reveal the protonation states of active site residues and bound inhibitor.[50] Supported by crystallographic analyses of ALR1 and ALR2,[54,55,31] in this study we demonstrate that whilst the anionic interaction in the active site of either enzyme can strongly anchor an inhibitor, it is an interaction that does not drastically influence ARI selectivity between the two enzymes given their homologous nature. This remains the domain of the hydrophobic contacts put upon the inhibitors at the C-terminal loop of the enzymes. Apart from the anionic binding site and Cys298, the active site of ALR2 is remarkably apolar and it marks the greatest difference from ALR1. In ALR1, Arg312 and Asp313 contribute greatly to the overall enthalpic component of inhibitor binding with compounds containing electronegative moieties such as halides and carboxylates.[39] In our modelling and analyses of ALR2, the inhibitor DCL fails to make a stabilizing contact similar to that with Arg312 in ALR1, with the Cl atoms at the 3- and 5-positions of the benzene ring being in almost direct conflict with the apolar residues of Val47, Phe121 and Phe122, suggesting that the carboxylate group is almost the sole contributor to the weaker inhibition of the enzyme. However, ALR2 does show significant competitive inhibition with phenyl acetic acid-based inhibitors[58], such as those with halide substituents at the 2- and 6-positions (PDB code 2IS7) pointing towards the anionic-binding site and Cys298, thus avoiding any possible steric conflicts with the hydrophobic residues. In the crystal structure of ALR1 bound to Tolrestat[31], it was shown that to accommodate the trifluoro group of the inhibitor the side chain conformation of Arg312 changes and that a Arg312Ala mutant of ALR1 improves the potency of the inhibitor indicating that Arg312 is another important determinate of inhibitor selectivity for ALR2 over ALR1.

With a predominantly hydrophobic active site, the largest measurable interactions were observed between the apolar residues of the ALR2 active site and inhibitor. These overall enthalpic contributions increase with the measured in vitro potency of the inhibitor (Tolrestat > Minalrestat > quercetin). In crystal structures of ALR2, it has been observed that a number of hydrophobic residues display different side chain conformations,[35,55,59] in particular Leu300, which in ALR1 is replaced with proline. The predominant contribution of this residue to inhibitor selectivity has been the hydrogen bond present between its main chain nitrogen and the ARI, particularly in the case of ALR2-Minalrestat (and another cyclic imide fidarestat[35]) crystal structure, an interaction not afforded by Pro301 in ALR1. In our modelling studies of quercetin we observed that the enthalpic interaction of this ARI with ALR2 was affected by the conformation of Leu300 and its proximity to the 3,4-dihydroxyphenyl moiety, which in turn altered the efficient π stacking interaction with Trp111. We did not observe a hydrogen bond interaction between Leu300 and the 3,4-dihydroxyphenyl moiety of quercetin, which is immediately surrounded by Phe122 and Phe115, and present within 4 Å of the side chain of Leu300, suggesting that hydrophobic interactions are the main contributors to inhibitor potency.

4. Conclusion

Our comparative inhibitor modelling and binding studies suggest that, whilst the H-bonding interactions between the polar heads of the inhibitors and the residues lining the anionic-binding site are conserved and contribute equally to inhibitor binding, additional non-conserved contacts are responsible for the difference in inhibitor potencies for ALR2 and ALR1. In particular, Arg312 in ALR1 (missing in ALR2) forms an electrostatic interaction with DCL and undergoes a conformational change upon binding of Tolrestat. These interactions contribute to stronger binding to ALR1 in case of DCL and weaker binding in case of Tolrestat. Thr113 in ALR2 (Tyr116 in ALR1) forms an electrostatic interaction with the fluorobenzyl moiety of Minalrestat which in turn π stacks against the side chain of Trp111. In the ALR1 model, the bulky side chain of the Tyr116 does not hold the fluorobenzyl moiety in place and the π stacking interaction with the Trp is missing. The fact that a correlation between the binding energy and IC_{50} value is not evident in this case suggests that a conformational change may occur upon the binding of Minalrestat including a change in the side chain conformation of Tyr116, allowing for a π stacking (3.8 Å) interaction to occur between the fluorobenzyl moiety and Trp114 (Fig. 3 and Table 1), similar to the one seen in ALR2. Attempts are currently underway to determine the crystal structure of ALR1 in complex with Minalrestat to obtain a more detailed picture of the inhibitor's binding conformation. In the case of quercetin, the additional H-bonding interactions with Thr113 contribute to the favourable binding and improved inhibitor potency for ALR2 over ALR1.

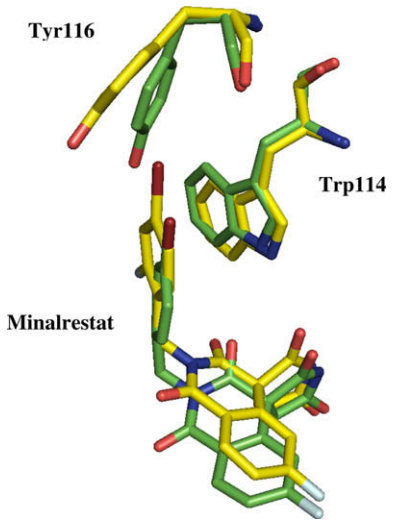

Figure 3. Superimposition showing the interaction between Tyr116 and Trp114 in ALR1 and Minalrestat with (yellow) and without (green) the proposed conformational change in the side chain of Tyr116 that results in the π stacking between the fluorobenzyl moiety of Minalrestat and Trp114. Figure was prepared after energy minimisation.

5. Experimental

5.1. Materials

Coenzyme (NADPH) and chemicals of the highest purity were purchased from the Sigma–Aldrich Chemical Company, Fluka and MERCK.

5.2. Purification of porcine ALR1

ALR1 was purified from porcine kidney utilising a previously published procedure.[33] Briefly, porcine kidneys were diced and homogenised in 10 mM sodium phosphate (pH 7.0) containing 5 mM 2-mercaptoethanol and 5 mM EDTA (buffer A). The homogenate was centrifuged, and the proteins in the supernatant were fractionated by adding ammonium sulfate (35% and 65% saturation). The pellet was resuspended in buffer A and purified by successive column chromatography including affinity Blue Sepharose, anionic exchange Q-Sepharose and gel filtration Superdex 75 (Pharmacia). The purified and desalted enzyme was stored in 5 mM Tris–HCl (pH 6.5) buffer containing 5 mM 2-mercaptoethanol.

5.3. Expression and purification of recombinant human ALR2

Plasmid construction, bacterial cell expression and protein purification were carried out using previously described protocols.[49] Briefly, the bacterial cells transfected with the expression plasmids were cultured in a Luria–Bertani medium and the expression of recombinant ALR2 was induced by the addition of 1 mM isopropyl 1-thio-β-D-galactopyranoside. The cells were collected, lysed and centrifuged. The supernatant fraction was immediately applied to a Sephadex G-75 column equilibrated with 20 mM imidazole–HCl (pH 7.2) containing 7 mM 2-mercaptoethanol. The enzyme fractions were applied to a MonoP column equilibrated with the imidazole buffer, and eluted with 1:10 diluted Polybuffer 74 (Pharmacia) containing 7 mM 2-mercaptoethanol. Active fractions were pooled, concentrated and dialysed against the imidazole buffer. The dialysed protein was then finally applied to a Blue Sepharose column, and eluted with a linear gradient of 0–1 M NaCl.

5.4. Assay of enzyme activity

Enzyme activity was measured by monitoring the decrease in NADPH absorbance at 340 nm and maintained at 298 K. The final reaction mixture for ALR2 activity consisted of 50 mM potassium phosphate (pH 6.2), 0.1 mM NADPH, 5 mM DL-glyceraldehyde, 5 mM 2-mercaptoethanol and 0.4 mM lithium sulfate in a total volume of 1.0 mL. The activity of ALR1 was determined in 50 mM potassium phosphate buffer (pH 6.7) containing only NADPH and the substrate. The inhibitors were dissolved in dimethyl sulfoxide, and added into the reaction mixture, in which the final concentration of dimethyl sulfoxide was less than 1.5%. The IC_{50} values were estimated from non-linear regression analyses of percent inhibition versus inhibitor concentration graphs and expressed as the means of at least three determinations. The inhibition pattern was analysed by fitting the initial velocities determined using variable concentrations of DL-glyceraldehyde in the Lineweaver–Burk plot.

5.5. Molecular modelling

To relieve any steric hindrance of the ARIs superimposed in the corresponding active sites, ALR2 complexed with quercetin and DCL, and ALR1 complexed with Minalrestat and quercetin, the models were subjected to energy minimisation. Taking into account inter-atomic van der Waals distances, initially the side chain conformations of amino acid residues were manually adjusted to a minimum to accommodate each superimposed inhibitor where necessary in order to conserve the conformational aspects of inhibitor binding. Energy minimisation was carried out using the DISCOVER 2.7 program (Biosym Technologies, San Diego, California, USA) on a Linux workstation following published protocols found to be effective for visualising a protein-ligand complex in its lowest energy conformation.[60,61] Briefly, calculations including a constant-valence force field incorporating the simple harmonic function for bond stretching and excluding all non-diagonal terms were carried out (cut-off distance of 26 Å) using the steepest-descent and conjugate-gradient algorithms (down to a maximum atomic root-mean-square derivative of 10.0 kcal/Å and 0.01 kcal/Å, respectively). Force–field potentials and partial charges were automatically assigned and visualised using InsightII, with the contributions of the proposed residues to the binding of inhibitor calculated using Discover. Additionally, the crystal structures of ALR2 containing Minalrestat and Tolrestat (PDB codes 1PWL and 2FZD) and ALR1 containing Tolrestat and DCL (PDB codes 3CV7) were used to extract the contribution of the active-site residues towards inhibitor binding.

References and notes

1. Zimmet, P.; Alberti, K. G. M. M.; Shaw, J. *Nature* **2001**, *414*, 782.
2. Oates, P. J. *Curr. Drug Targets* **2008**, *9*, 14.
3. Oates, P. J. *Int. Rev. Neurobiol.* **2002**, *50*, 325.
4. Reddy, G. B.; Satyanarayana, A.; Balakrishna, N.; Ayyagari, R.; Padma, M.; Viswanath, K.; Petrash, J. M. *Mol. Vis.* **2008**, *14*, 593.
5. Lee, A. Y.; Chung, S. K.; Chung, S. S. *Proc. Natl. Acad. Sci. U.S.A.* **1995**, *92*, 2780.
6. Jay, D.; Hitomi, H.; Griendling, K. K. *Free Rad. Biol. Med.* **2006**, *40*, 183.
7. Sato, S. *Am. J. Physiol.* **1992**, *263*, F799.
8. Wermuth, B.; Munch, J. D.; von Wartburg, J. P. *J. Biol. Chem.* **1977**, *252*, 3821.
9. Tabakoff, B.; Erwin, V. G. *J. Biol. Chem.* **1970**, *245*, 3263.
10. Tulsiani, D. R.; Touster, O. *J. Biol. Chem.* **1977**, *252*, 2545.
11. Flynn, T. G.; Shires, J.; Walton, D. J. *J. Biol. Chem.* **1975**, *250*, 2933.
12. Narayanan, S. *Ann. Clin. Lab. Sci.* **1993**, *23*, 148.
13. Hung, C. F.; Penning, T. M. *Mol. Endocrinol.* **1999**, *13*, 1704.
14. Nelson, V. L.; Qin, K. N.; Rosenfield, R. L.; Wood, J. R.; Penning, T. M.; Legro, R. S.; Strauss, J. F., III; McAllister, J. M. *J. Clin. Endocrinol. Metab.* **2001**, *86*, 5925.
15. Gavidia, I.; Perez-Bermudez, P.; Seitz, H. U. *Eur. J. Biochem.* **2002**, *269*, 2842.
16. Steckelbroeck, S.; Jin, Y.; Oyesanmi, B.; Kloosterboer, H. J.; Penning, T. M. *Mol. Pharmacol.* **2004**, *66*, 1702.
17. Ji, Q.; Aoyama, C.; Nien, Y. D.; Liu, P. I.; Chen, P. K.; Chang, L.; Stanczyk, F. Z.; Stolz, A. *Cancer Res.* **2004**, *64*, 7610.

18. Kanazu, T.; Shinoda, M.; Nakayama, T.; Deyashiki, Y.; Hara, A.; Sawada, H. *Biochem. J.* **1991**, *279*, 903.
19. Feather, M. S.; Flynn, T. G.; Munro, K. A.; Kubiseski, T. J.; Walton, D. J. *Biochim. Biophys. Acta* **1995**, *1244*, 10.
20. Ratliff, D. M.; Vander Jagt, D. J.; Eaton, R. P.; Vander Jagt, D. L. *J. Clin. Endocrinol. Metab.* **1996**, *81*, 488.
21. Sawada, H.; Hara, A.; Nakayama, T.; Hayashibara, M. *J. Biochem. (Tokyo)* **1982**, *92*, 185.
22. Takahashi, M.; Fujii, J.; Teshima, T.; Suzuki, K.; Shiba, T.; Taniguchi, N. *Gene* **1993**, *127*, 249.
23. Hara, A.; Deyashiki, Y.; Nakayama, T.; Sawada, H. *Eur. J. Biochem.* **1983**, *133*, 207.
24. Sawada, H.; Hara, A.; Nakayama, T.; Kato, F. *J. Biochem. (Tokyo)* **1980**, *87*, 1153.
25. Bohren, K. M.; Grimshaw, C. E.; Gabbay, K. H. *J. Biol. Chem.* **1992**, *267*, 20965.
26. El-Kabbani, O.; Judge, K.; Ginell, S. L.; Myles, D. A.; DeLucas, L. J.; Flynn, T. G. *Nat. Struct. Biol.* **1995**, *2*, 687.
27. Foppiano, M.; Lombardo, G. *Lancet* **1997**, *349*, 399.
28. Dhagat, U.; Endo, S.; Hara, A.; El-Kabbani, O. *Bioorg. Med. Chem.* **2008**, *16*, 3245.
29. El-Kabbani, O.; Wilson, D. K.; Petrash, M.; Quiocho, F. A. *Mol. Vis.* **1998**, *4*, 19.
30. Sato, S.; Kador, P. F. *Biochem. Pharmacol.* **1990**, *40*, 1033.
31. El-Kabbani, O.; Carper, D. A.; McGowan, M. H.; Devedjiev, Y.; Rees-Milton, K. J.; Flynn, T. G. *Proteins* **1997**, *29*, 186.
32. El-Kabbani, O.; Old, S. E.; Ginell, S. L.; Carper, D. A. *Mol. Vis.* **1999**, *5*, 20.
33. El-Kabbani, O.; Rogniaux, H.; Barth, P.; Chung, R. P.; Fletcher, E. V.; Van Dorsselaer, A.; Podjarny, A. *Proteins* **2000**, *41*, 407.
34. El-Kabbani, O.; Ramsland, P.; Darmanin, C.; Chung, R. P.; Podjarny, A. *Proteins* **2003**, *50*, 230.
35. El-Kabbani, O.; Darmanin, C.; Schneider, T. R.; Hazemann, I.; Ruiz, F.; Oka, M.; Joachimiak, A.; Schulze-Briese, C.; Tomizaki, T.; Mitschler, A.; Podjarny, A. *Proteins* **2004**, *55*, 805.
36. Wilson, D. K.; Tarle, I.; Petrash, J. M.; Quiocho, F. A. *Proc. Natl. Acad. Sci. U.S.A.* **1993**, *90*, 9847.
37. Urzhumtsev, A.; Tête-Favier, F.; Mitschler, A.; Barbanton, J.; Barth, P.; Urzhumtseva, L.; Biellmann, J. F.; Podjarny, A.; Moras, D. A. *Structure* **1997**, *5*, 601.
38. Bohren, K. M.; Grimshaw, C. E.; Gabbay, K. H. *J. Biol. Chem.* **1992**, *267*, 20965.
39. Barski, O. A.; Gabbay, K. H.; Bohren, K. M. *Biochemistry* **1996**, *35*, 14276.
40. Jez, J. M.; Flynn, T. G.; Penning, T. M. *Biochem. Pharmacol.* **1997**, *54*, 639.
41. Warren, J. C.; Murdock, G. L.; Ma, Y.; Goodman, S. R.; Zimmer, W. E. *Biochemistry* **1993**, *32*, 1401.
42. Dixit, B. L.; Balendiran, G. K.; Watowich, S. J.; Srivastava, S.; Ramana, K. V.; Petrash, J. M.; Bhatnagar, A.; Srivastava, S. K. *J. Biol. Chem.* **2000**, *275*, 21587.
43. Srivastava, S. K.; Ramana, K. V.; Bhatnagar, A. *Endocr. Rev.* **2005**, *26*, 380–392.
44. Srivastava, S.; Watowich, S. J.; Petrash, J. M.; Srivastava, S. K.; Bhatnagar, A. *Biochemistry.* **1999**, *38*, 42.
45. Srivastava, S.; Spite, M.; Trent, J. O.; West, M. B.; Ahmed, Y.; Bhatnagar, A. J. *Biol. Chem.* **2004**, *279*, 53395.
46. Hayashi, H.; Fujii, Y.; Watanabe, K.; Urade, Y.; Hayaishi, O. *J. Biol. Chem.* **1989**, *264*, 1036.
47. Bhatnagar, A.; Liu, S. Q.; Das, B.; Ansari, N. H.; Srivastava, S. K. *Biochem. Pharmacol.* **1990**, *39*, 1115.
48. Costantino, L.; Rastelli, G.; Gamberini, M. C.; Vinson, J. A.; Bose, P.; Iannone, A.; Staffieri, M.; Antolini, L.; Del Corso, A.; Mura, U.; Albasini, A. *J. Med. Chem.* **1999**, *42*, 1881.
49. Hohman, T. C.; El-Kabbani, O.; Malamas, M. S.; Lai, K.; Putilina, T.; McGowan, M. H.; Wane, Y. Q.; Carper, D. A. *Eur. J. Biochem.* **1998**, *256*, 310.
50. Podjarny, A.; Cachau, R. E.; Schneider, T.; Van Zandt, M.; Joachimiak, A. *Cell. Mol. Life Sci.* **2004**, *61*, 763.
51. Steuber, H.; Czodrowski, P.; Sotriffer, C. A.; Klebe, G. *J. Mol. Biol.* **2007**, *373*, 1305.
52. Harrison, D. H.; Bohren, K. M.; Ringe, D.; Petsko, G. A.; Gabbay, K. H. *Biochemistry.* **1994**, *33*, 2011.
53. Bohren, K. M.; Grimshaw, C. E.; Lai, C. J.; Harrison, D. H.; Ringe, D.; Petsko, G. A.; Gabbay, K. H. *Biochemistry* **1994**, *33*, 2021.
54. Carbone, V.; Chung, R.; Endo, S.; Hara, A.; El-Kabbani, O. *Arch. Biochem. Biophys.* **2008**, *479*, 82.
55. Steuber, H.; Zentgraf, M.; Gerlach, C.; Sotriffer, C. A.; Heine, A.; Klebe, G. *J. Mol. Biol.* **2006**, *363*, 174.
56. Drel, V. R.; Pacher, P.; Ali, T. K.; Shin, J.; Julius, U.; El-Remessy, A. B.; Obrosova, I. G. *Int. J. Mol. Med.* **2008**, *21*, 667.
57. El-Kabbani, O.; Green, N. C.; Lin, G.; Carson, M.; Narayana, S. V.; Moore, K. M.; Flynn, T. G.; DeLucas, L. J. *Acta Crystallogr., Sect. D: Biol. Crystallogr.* **1994**, *50*, 859.
58. Brownlee, J. M.; Carlson, E.; Milne, A. C.; Pape, E.; Harrison, D. H. *Bioorg. Chem.* **2006**, *34*, 424.
59. Steuber, H.; Heine, A.; Podjarny, A.; Klebe, G. *J. Mol. Biol.* **2008**, *379*, 991.
60. Darmanin, C.; El-Kabbani, O. *Bioorg. Med. Chem. Lett.* **2001**, *11*, 3133.
61. Darmanin, C.; El-Kabbani, O. *Bioorg. Med. Chem. Lett.* **2000**, *10*, 1101.
62. DeLano, W. L. *The PyMOL Molecular Graphics System*; DeLano Scientific: San Carlos, CA, 2002.